Vol. 40 — N° 3 09 16 P. 351 – 363

GEOSTANDARDS and GEOANALYTICAL RESEARCH

A Practical Method for Accurate Measurement of Trace Level Fluorine in Mg- and Fe-Bearing Minerals and Glasses Using Electron Probe Microanalysis

Chao **Zhang** (1)*, Jürgen **Koepke** (1), Lian-Xun **Wang** (2), Paul E. **Wolff** (1), Sören **Wilke** (1), André **Stechern** (1), Renat **Almeev** (1) and Francois **Holtz** (1)

(1) Institut für Mineralogie, Leibniz Universität Hannover, Callinstraße 3, Hannover, 30167, Germany
(2) School of Earth Sciences, China University of Geosciences, Wuhan, 430074, China
* Corresponding author. e-mail: c.zhang@mineralogie.uni-hannover.de

Fluorine plays an important role in magmatic and hydrothermal processes, but due to its low abundance in geological samples determining F is difficult by electron probe microanalysis. By using a W-Si multi-layered pseudocrystal as the diffraction crystal instead of thallium acid phthalate (TAP), count rates were considerably higher, which however introduced spectral interferences between F*Kα* and Fe*Lα* and Mg*Kβ* lines when normal integral mode is applied. In this study, we developed a protocol using a W-Si multi-layered pseudocrystal for measuring accurately trace level F in both minerals and glasses. First, we used differential mode with an optimised PHA (pulse height analysis) setting in signal processing, instead of normal integral mode, which completely eliminated the second-order Mg*Kβ* line. Second, the overlap of the first-order Fe*Lα* on F*Kα* peak, which cannot be filtered by modifying the PHA setting, was calibrated quantitatively using F-free minerals and silicate glasses. Applying this two-step method, F was determined in a number of reference glasses, as well as in glasses synthesised from powders of the rock reference materials AC-E, GS-N and DR-N. Our data are consistent within error with F concentrations determined by other methods, demonstrating the reliability of this method.

Keywords: electron probe microanalysis, *in situ* techniques, reference materials, microbeam techniques, wavelength dispersive X-ray fluorescence spectrometry.

Le Fluor joue un rôle important dans les processus magmatiques et hydrothermaux mais l'analyse quantitative de cet élément dans les phases solides par microsonde électronique reste difficile. Le taux de comptage peut être augmenté de manière significative en utilisant un pseudocristal de W-Si au lieu de thallium acid phthalate (TAP). Cependant, l'utilisation de W-Si entraine des interférences spectrales des lignes Fe*Lα* et Mg*Kβ* avec F*Kα*, ce qui introduit des difficultés pour la détermination de la position exacte à choisir pour la mesure du pic de F*Kα* et du bruit de fond. Afin de quantifier le rôle de ces interférences, nous proposons un protocole pour l'analyse du fluor dans des verres et des minéraux avec W-Si. Nous avons utilisé le mode différentiel pour le traitement du signal et optimisé la valeur de PHA (pulse height analysis), ce qui permet d'éliminer totalement la raie de second ordre de Mg*Kβ* et par conséquent les interférences spectrales avec la ligne Mg*Kβ*. L'optimisation de PHA ne permet cependant pas de supprimer totalement la raie Fe*Lα*. Nous avons donc effectué une série de mesures dans des verres et dans des phases solides dépourvus de Fluor pour calibrer les interférences spectrales avec la ligne Fe*Lα*. Nous avons appliqué cette méthode pour l'analyse du Fluor dans des verres à teneurs en Fluor connues. En tenant compte de l'erreur de mesure, les teneurs en Fluor déterminées sont identiques aux valeurs de référence. Il est important de souligner que la correction à appliquer pour tenir compte des interférences spectrales avec la ligne Fe*Lα* dépend de la valeur de PHA, du courant du faisceau, de la nature du matériel analysé (verre, minéral) et probablement d'autres conditions analytiques. Il est donc recommandé de procéder périodiquement à une recalibration pendant chaque session analytique.

doi: 10.1111/j.1751-908X.2015.00390.x

GEOSTANDARDS and GEOANALYTICAL RESEARCH

Mots-clés : microsonde électronique, techniques in situ, matériaux de référence, techniques de microfaisceaux, longueur d'onde de dispersion, rayons X spectrométrie de fluorescence.

Received 07 Sep 15 – Accepted 14 Dec 15

Fluorine (F) is an important volatile element in magmatic and hydrothermal processes despite usually occurring at trace levels in major rock-forming minerals and glasses. Fluorine is highly soluble in silicate melts, and it may behave as an incompatible element in common rhyolitic systems when minerals crystallise and/or fluids are exsolved (e.g., Webster 1990), or become enriched in fluids relative to silicate melts in basaltic and phonolitic systems (e.g., Chevychelov *et al.* 2008a, b). As a result, F may behave as a major element in high-silica residual liquids resulting from extreme crystallisation in pegmatitic systems, in systems that have undergone high-temperature alteration (e.g., greisens, metasomatic rocks) and in veins precipitated from hydrothermal fluids. Fluorine-rich minerals (e.g., topaz, fluorite, cryolite) may crystallise from such high-F systems (e.g., Webster *et al.* 1987). In crystalline rocks formed in common magmatic and hydrothermal systems, F normally occurs at trace levels (in most cases < 1% *m/m*, i.e., mass/mass) and is mainly stored in hydrous minerals such as apatite, mica and amphibole via substitution with hydroxyl. In addition, F can also be incorporated into nominally anhydrous minerals such as olivine, pyroxene, garnet and plagioclase at high pressures via oxygen defects (e.g., Beyer *et al.* 2012, Le Voyer *et al.* 2014). For research on geological samples composed of different phases (such as minerals, glass matrix and melt inclusions) with very small sizes and/or inhomogeneous distribution of F, *in situ* accurate determination of F is required to reveal the systematics of its distribution.

Due to the ease of access to electron microprobe instruments compared with SIMS instruments, it is important to develop an accurate and reliable analytical method using EPMA to determine trace levels of F in natural minerals and glasses. The property of analytical crystals has a dominant influence on the count rate. The conventional TAP crystal has an interplanar spacing (*d*) of 12.95 Å with a low count rate for F*K*α X-rays, resulting in a high detection limit and a large analytical error (Potts and Tindle 1989). With the use of the synthetic W-Si multi-layered pseudocrystal (termed LDE1 by JEOL and PC1 by CAMECA), which has a large *d* value of 30 Å, much higher count rate for low atomic number elements can be obtained (Anzelmo and Boyer 1987, Potts and Tindle 1989, Witter and Kuehner 2004). For example, by measuring the F content of a synthetic SrF_2 crystal using a CAMECA SX100 instrument, we obtained F count rates of *ca.* 13 and 390 cps/nA (counts per second per nA) using TAP and PC1 crystals respectively, showing a substantial improvement of the count rate by a factor of 30 when using the PC1 pseudocrystal. However, with the PC1 pseudocrystal, there are small but significant spectral interferences of the F*K*α peak with Fe- and Mg-induced X-ray lines (Potts and Tindle 1989), which cannot be ignored when analysing trace level F in Fe- and Mg-bearing materials (Donovan *et al.* 1993, Witter and Kuehner 2004). Such interferences have been very often overlooked in numerous studies that utilised EPMA for determining F contents in Mg- and Fe-bearing phases, such as amphibole, biotite and glass inclusions. In this paper, we present a two-step method for determining trace level F (hundreds to thousands of $\mu g\ g^{-1}$) in Mg- and Fe-bearing phases by EPMA using the PC1 pseudocrystal. This method was tested by measuring a number of international reference materials.

Experimental procedures

Theoretical background

As shown by the spectral scan of the international reference mineral Kakanui Hornblende (USNM 143965) (see Jarosewich *et al.* 1980) using the commonly used integral mode in X-ray signal processing (integral mode in Figure 1a), it is evident that adjacent to the F*K*α line (peak position at sin θ = 0.30905) there are first-order Fe*L*β and Fe*L*α (*n* = 1) lines on the left side, and second-order Mg*K*α and Mg*K*β (*n* = 2) lines on the right side. Comparison of Figures 1a and b (spectral scan of the Durango Fluorapatite, F content 3.35% *m/m*, Marks *et al.* 2012) indicates that the Fe*L*α line overlaps at the peak position of the F*K*α, while the Mg*K*β line overlaps at the right-side background position of the of the F*K*α. Table 1 lists the X-ray lines induced by Fe and Mg adjacent to the F*K*α peak, which were detected using the CAMECA SX100 electron probe micro analyser equipped with a PC1 pseudocrystal at the Institute of Mineralogy, Leibniz University of Hannover. We note that the interplanar spacing of the PC1 pseudocrystal was calculated as 29.639 Å, slightly less than the ideal value of 30 Å.

A few studies have been dedicated to calibrating quantitatively the spectral interferences of F*K*α with Fe- and

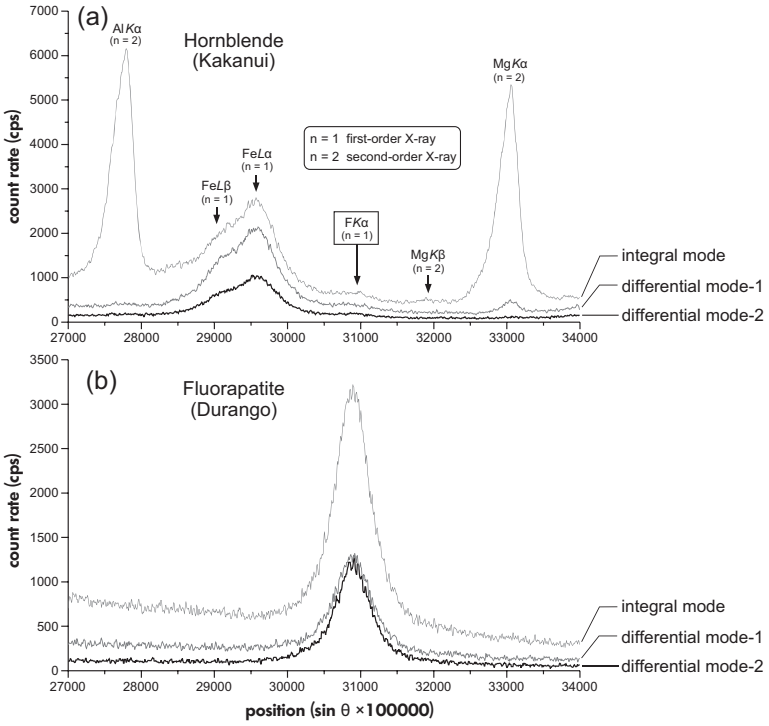

Figure 1. Spectral scans with modification in pulse height analysis setting. (a) Hornblende Kakanui (USNM 143965). (b) Fluorapatite Durango (USNM 104021). Integral mode, baseline = 1800 mV. Differential mode-1, baseline = 1800 mV, window = 3000 mV. Differential mode-2, baseline = 2800 mV, window = 1100 mV. Note that the F*K*α, Fe*L*β and Fe*L*α lines are first-order (*n* = 1), and the Mg*K*α, Mg*K*β and Al*K*α lines are second-order (*n* = 2). The comparison between (a) and (b) indicates that the FeLα line overlaps at the peak position of the F*K*α, while the Mg*K*β line overlaps at the right-side background position of the of the F*K*α. Using differential mode-1 instead of integral mode strongly diminishes Mg*K*α and Mg*K*β as well as F*K*α, and using differential mode-2 instead of differential mode-2 eliminates completely Mg*K*α and Mg*K*β but does not depress F*K*α. Therefore, differential mode-2 is an optimal setting for analysing F*K*α intensity without overlap from Mg. Scan setting: beam current 180 nA, beam size 5 μm, dwell time 0.1 s, accumulation number 5.

Table 1.
Summary of X-ray lines adjacent to F*K*α peak

Element	Line	Order	λ (Å)	Position (sin θ)
F	*K*α	1st	18.3200	0.30905
Fe	*L*α	1st	17.5900	0.29543
Fe	*L*β	1st	17.2600	0.29133
Mg	*K*α	2nd	19.7800	0.33055
Mg	*K*β	2nd	19.0420	0.31948

The sin θ values were detected using a CAMECA SX100 electron probe (Institute of Mineralogy, Leibniz University of Hannover) equipped with a PC1 pseudocrystal. Based on the F*K*α peak position of sin θ = 0.30905, the real interplanar spacing of the diffraction crystal PC1 was calculated as 29.639 Å, applying the equation $\lambda = 2d \sin\theta$, in which λ is wavelength, d is interplanar spacing of the diffraction crystal. The ideal positions for d = 30 Å can be found at http://geoloweb.ch/cub/index.php.

Mg-induced X-ray lines. By measuring fayalite and magnesium oxide, Potts and Tindle (1989) reported the interferences by means of correction factors from Fe and Mg on determined F concentrations. Donovan *et al.* (1993) used magnetite to calibrate the interference with Fe*L*α in determining F, but ignored Mg. Unfortunately, the measurement protocols (e.g., background position) in both studies were not clearly documented, and analyses were not confirmed by measurements of any known F-bearing and Fe- and Mg-bearing reference materials. Using several Fe-bearing F-free RMs, Witter and Kuehner (2004) calibrated the interference with Fe*L*α by measuring counts both at the F*K*α peak (sin θ = 0.29857) and at a nearby right-side background position (sin θ = 0.30571), and proposed a correction method to be used for determining F in Mg- and Fe-bearing materials. However, the accuracy of this method may be questioned due to two potential sources of error that were not taken into account by the authors. First, because of the broad width of F*K*α peak, the position of measured background is too close to the F*K*α peak and thus the method underestimates the background-corrected F*K*α peak counts. Second, the measured background is located

between the F*K*α and Mg*K*β peaks, but the potential interference from Mg on the background was ignored. In this study, we designed and thoroughly tested a new two-step method, which (a) eliminates the second-order Mg*K*β line on the right-side background of the F*K*α peak and (b) calibrates the interference of Fe*L*α line at the position of the F*K*α peak.

Eliminating Mg overlap

During signal processing by wavelength dispersive X-ray spectroscopy (WDS), X-ray lines with similar wavelength but different energy can be filtered using PHA with differential mode. By pre-setting the baseline and window values, only the predetermined signal voltage range (from base line to baseline + window) is used for WDS output (see details in Goldstein *et al.* 1981). Setting PHA with the differential mode, instead of the commonly used integral mode, has been usually applied to eliminate signals from overlapping elements for accurate determination of trace elements (e.g., Fialin *et al.* 1999, Jercinovic and Williams 2005). In this study, because the second-order Mg X-ray lines have energies higher than the first-order F*K*α by a factor of 2, setting a proper PHA can eliminate the Mg X-ray lines that overlap with the right-side background of F*K*α. This method was not applied in the former F analytical studies (Potts and Tindle 1989, Witter and Kuehner 2004). As indicated by the spectral scans for the Kakanui Hornblende (Figure 1a), using the differential mode-1 (baseline = 1800 mV, window = 3000 mV) instead of the integral mode (baseline = 1800 mV) can strongly depress the second-order Mg*K*α and Mg*K*β lines (and Al*K*α as well). Note, however, that the application of the differential mode also leads to a decrease of the signal intensities of the first-order F*K*α line as indicated by the spectral scans for the Durango Fluorapatite (Figure 1b). Further, using the differential mode-2 (baseline = 2800 mV, window = 1100 mV) instead of the differential mode-1 can completely diminish the second-order Mg X-ray lines (Figure 1a), but does not apparently decrease the intensity of F*K*α (Figure 1b). Therefore, the setting of differential mode-2 is optimal for eliminating the Mg overlap when analysing the F*K*α signal and has been used for all the calibration and measurements presented below.

Quantifying Fe overlap

Because the first-order Fe*L*α line overlapping with the F*K*α cannot be eliminated by setting PHA (Figure 1a), the interference must be quantitatively calibrated in terms of FeO(T) content (total iron expressed as FeO) for an accurate analysis the F*K*α signal. Figures 2a and b compare the spectral scans of F-free olivine (Fo_{83}, FeO(T) 16.4% *m/m*) and anorthite (FeO (T) 0.4% *m/m*) as well as F-bearing phases (Kakanui Hornblende and the rhyolitic glass). Comparison of the spectral scans show that an interference of the Fe X-ray lines with the F*K*α peak occurred. Because the interference of the Mg*K*β line with the F*K*α line was eliminated via setting PHA, and because the F*K*α line overlapped with the Fe X-ray lines (left side of the scans on Figure 2), we propose to use a background value at the position sin θ = F*K*α peak + 0.01 where no interference occurred (i.e., 0.31905 in this case, Figure 2c). As illustrated in Figure 2c, the background at F*K*α peak (Bg_1) cannot be measured directly because of the contribution of Fe X-ray lines but can be calculated from the measured apparent background at the chosen right-side position of sin θ = F*K*α peak + 0.01 (Bg_2). The quantitative relation between Bg_1 and Bg_2 can be calibrated by measuring a number of known F-free minerals and glasses that contain various FeO(T) contents (X_{FeO}) (Table 2). Assuming that both backgrounds (Bg_1 and Bg_2) are functions of beam current, 'Bremsstrahlung', and correlate with X_{FeO} in a linear way, we can write the following equations:

$$Bg_1 = Q * (a_1 + b_1 * X_{FeO}) \quad (1)$$

$$Bg_2 = Q * (a_2 + b_2 * X_{FeO}) \quad (2)$$

where Q is a function of beam current, constants a_1 and a_2 account for the 'Bremsstrahlung', and the constants b_1 and b_2 take the X_{FeO} into account (linear relation). Note that these parameters do not need to be determined since they are integrated to other constants in the following equations (see below).

By measuring Bg_1 and Bg_2 of Fe-bearing but F-free materials, the analyses yield pseudo (or apparent) F concentrations (C^F_{Fe}), (see Figure 2c). Assuming that matrix correction can be ignored without a significant deviation, C^F_{Fe} can be calculated as

$$C^F_{Fe} = (Bg_1 - Bg_2)/(K * I) \quad (3)$$

where *K* is a conversion factor for calculating F concentration from counts and *I* is the beam current. Combining the above equations, we obtain

$$C^F_{Fe} = (a_1 - a_2) * \frac{Q}{K * I} + (b_1 - b_2) * \frac{Q}{K * I} * X_{FeO} \quad (4)$$

Assuming that

$$a = (a_1 - a_2) * Q/(K * I),\ b = (b_1 - b_2) * Q/(K * I) \quad (5)$$

we can finally obtain

$$C^F_{Fe} = a + b * X_{FeO} \quad (6)$$

The values of *a* and *b* can be determined by linear regression of a series of (C^F_{Fe}) and X_{FeO} values of measured

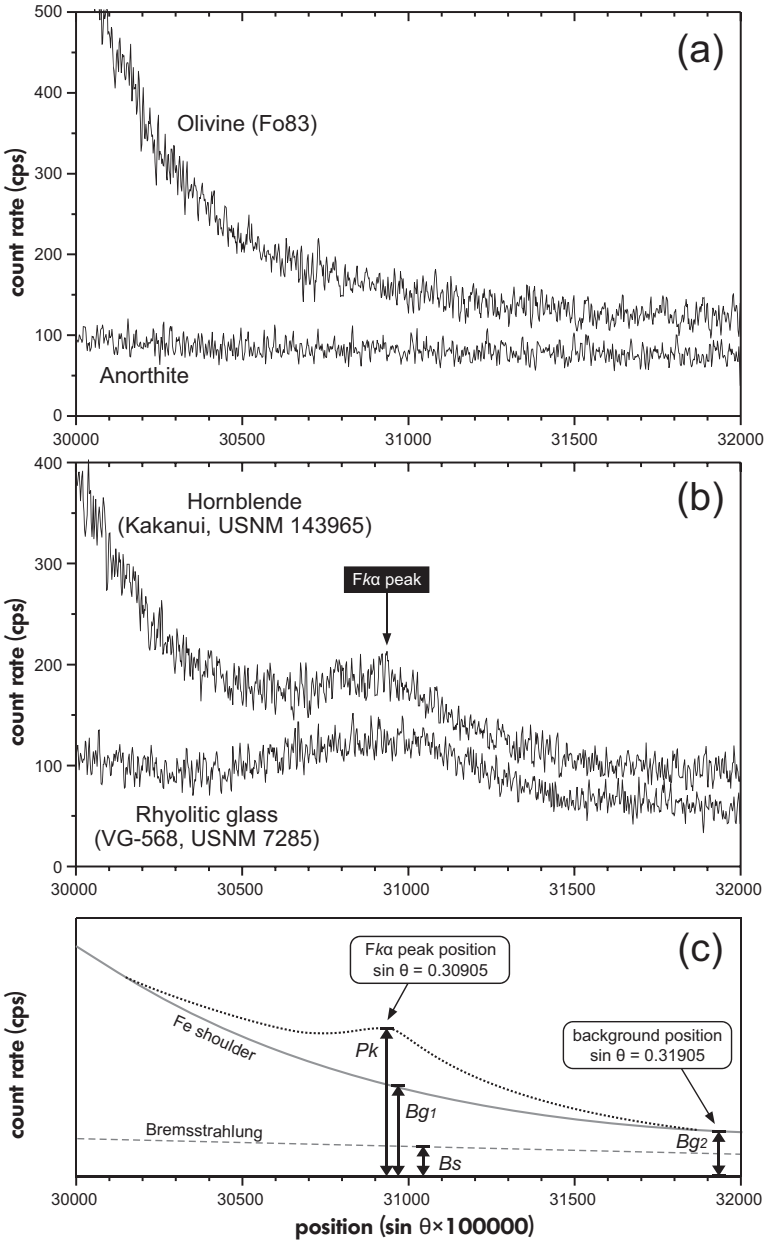

Figure 2. Overlap of F*K*α by the Fe shoulder. (a) F-free phases: Olivine (Fo83) and Anorthite. (b) F-bearing phases: Hornblende (Kakanui) and Rhyolitic glass (VG-568). (c) Working model for analysing F*K*α with background correction for the interference with the Fe shoulder. Note that the Mg*K*β line at sin θ = 0.31948 (see Table 1) was completely eliminated by using an optimised differential mode (differential mode-2 in Figure 1). In our calculation, *Pk* is measured counts at F*K*α peak, Bg_1 is theoretical background counts at F*K*α peak, Bg_2 is measured background counts for calibrating Bg_1, and *Bs* is counts derived from Bremsstrahlung. Spectral scan with differential mode, baseline = 2800 mV, window = 1100 mV. Scan setting: beam current 180 nA, beam size 5 μm, dwell time 0.1 s, accumulation number 5.

F-free materials. By using a fixed beam current, the function *Q*, which describes the effect of beam current on the signal intensities of Bg_1 and Bg_2, is thus a constant and does not require to be quantified.

In this study, three datasets for quantifying the relation between (C_{Fe}^{F}) and X_{FeO} were measured, which were derived from minerals using a beam current of 180 nA, glasses with a beam current of 60 nA, and minerals with a

beam current of 60 nA (Table 2). As plotted in Figure 3a, six anhydrous minerals (anorthite, omphacite, augite, pyrope, hypersthene and olivine) and two experimental F-free calcic amphiboles, measured with a beam current of 180 nA, exhibited a consistent linear relation. Figure 3b shows that the six experimental F-free glasses with a broad compositional range (rhyolite, phonolite, rhyodacite, andesite, high-Mg basalt, MOR basalt), measured with a beam current of 60 nA, yielded a good linear fit. Figure 3b also shows the plots of the six anhydrous minerals measured with a beam current of 60 nA, which indicate a fitted relation that differs strongly from that of minerals with a beam current of 180 nA, as well as from that of glasses with a beam current of 60 nA. First, the change of beam current resulted in a change of the relation between (C^F_{Fe}) and X_{FeO}, because the parameters *a* and *b* are functions of the beam current (see above). Second, the measurements of glasses and minerals using the same beam current showed distinctive individual relations, which are thought to be attributed to contrasting matrix effects. Therefore, the calibration of the relation between (C^F_{Fe}) and X_{FeO} must be performed for mineral or glass, separately, using a constant beam current.

For F-bearing materials, Bg_1 cannot be measured directly but can be calculated by measuring Bg_2 and using the relation between Bg_1 and Bg_2 derived from F-free materials described above. The measured raw F concentration (C^F_{mea}), which is converted from subtracting Bg_2 from *Pk*, is a combination involving both the real F concentration (C^F_{real}, corresponding to the counts of $Pk\text{-}Bg_1$) and the interference with Fe X-ray lines (C^F_{Fe} corresponding to the counts of $Bg_1\text{-}Bg_2$). Therefore, we can calculate C^F_{real} of unknown F-bearing materials from the equation

$$C^F_{real} = C^F_{mea} - C^F_{Fe} \quad (7)$$

Table 3 summarises the steps of the method for determining trace level F in Mg- and Fe-bearing minerals or glasses. The calibrated relation between C^F_{Fe} and X_{FeO} for minerals in Figure 3a should be valid for a broad range, including amphibole and other hydrous minerals (e.g., biotite), with FeO(T) of at least 0–16% *m/m*. The calibrated relation between (C^F_{Fe}) and X_{FeO} derived from a variety of glasses in Figure 3b is expected to be valid for a wide compositional range, with FeO(T) of at least 0–10% *m/m*, as shown by our test using reference glasses (see below and Table 4). This calibration should also be valid for glasses with moderately higher FeO(T).

However, we note that the calibrated C^F_{Fe} and X_{FeO} relation can vary not only with the nature of material (i.e., mineral or glass) and beam current, but also with other settings (e.g., baseline, window, bias, gain, etc.), which implies that the fitted equations shown in Figure 3 may not be valid in other

Table 2.
Compositions of F-free phases used for calibration

Beam current	Phases	X_{FeO} (% *m/m*)	*s* (% *m/m*)	C^F_{Fe} (μg g^{-1})	*s* (μg g^{-1})
180 nA	Anorthite	0.40	0.04	195	31
	Omphacite	4.58	0.13	448	45
	Augite	6.22	0.19	541	13
	Pyrope	10.05	0.22	663	23
	Hypersthene	15.09	0.16	880	11
	Olivine (Fo83)	16.44	0.19	980	39
	Amphibole-1	10.91	0.21	790	30
	Amphibole-2	13.80	0.54	928	27
60 nA	Anorthite	0.40	0.04	220	28
	Omphacite	4.59	0.11	387	70
	Augite	6.21	0.21	449	21
	Pyrope	10.05	0.21	557	42
	Hypersthene	14.92	0.13	673	32
	Olivine (Fo83)	16.41	0.29	729	20
	Rhyolite	1.02	0.18	77	47
	Phonolite	2.21	0.24	173	18
	Rhyodacite	3.60	0.14	257	47
	Andesite	7.06	0.14	515	32
	High-Mg basalt	7.56	0.27	533	16
	MOR basalt	9.33	0.24	667	52

C^F_{Fe} (pseudo F concentration as a result of spectral interferences from Fe shoulder, see text for detailed explanation) was measured with a counting time of 120 s at peak and 60 s at background. Minerals were analysed with a beam size of 5 μm, while glasses were analysed with a beam size of 10 μm. Analytical number was 10 for each sample. F-free amphiboles and glasses were synthesised in the experimental petrology laboratory of the Institute of Mineralogy (Leibniz University of Hannover), and the compositions are listed in online supporting information Table S1.

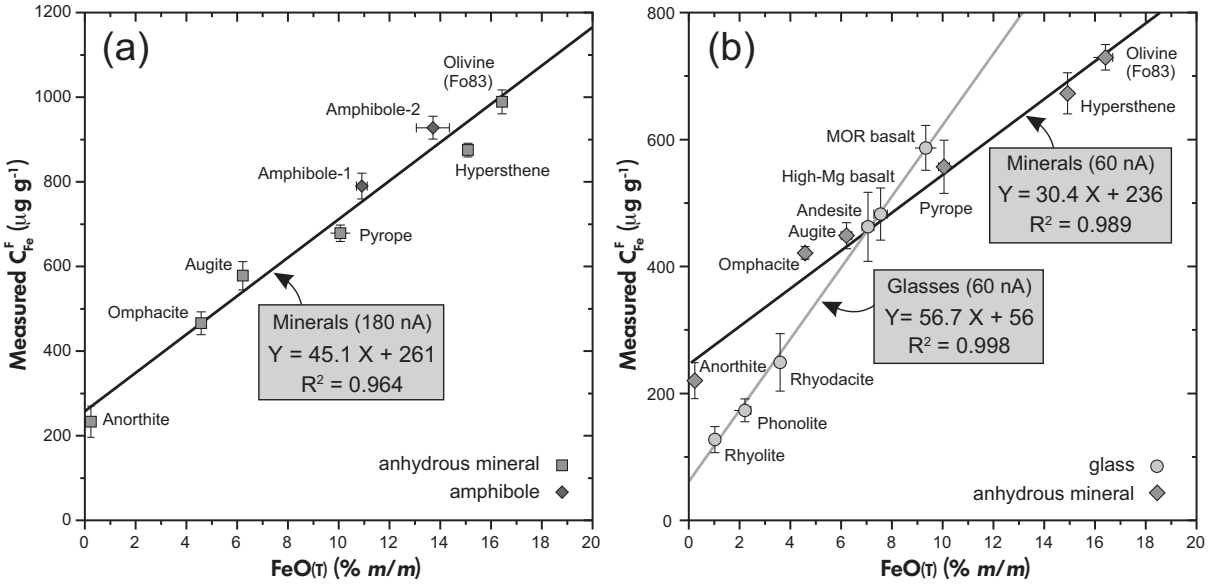

Figure 3. Relation between measured C^F_{Fe} and FeO(T) for background correction. (a) Relation in minerals analysed with a beam current of 180 nA. (b) Relation in glasses and minerals analysed with beam current of 60 nA. Also shown are linear regression lines and equations for C^F_{Fe} vs. FeO(T). Note that using the same beam current, the measured glasses and minerals showed significantly different relations between C^F_{Fe} and FeO(T). The data are listed in Table 2. It is noteworthy that the fitted equations shown here are only valid for analyses using the same pulse height analysis and beam settings as that applied in this study (see text for detailed explanation).

laboratories with a different instrument type or a different measurement setting. Therefore, to ensure the measurement accuracy, the calibration for C^F_{Fe} and X_{FeO} should be periodically performed during each measurement session.

Analytical setting

The analytical method presented in this paper was performed and tested using a CAMECA SX100 instrument at the Institute of Mineralogy, Leibniz University of Hannover (Germany). All analyses were performed with a 15 kV operation voltage and the 'PAP' matrix correction after Pouchou and Pichoir (1991). The diffracting crystals used were: PC1 for F; LPET for K, Ti, and Cl; TAP for Na, Mg, Si, and Al; PET for Ca; LIF for Fe and Mn. For determining major elements in minerals, a beam current of 15 nA was used, whereas for determining major elements in glasses, a reduced beam current of 8 nA was used. Determinations of Cl and F were performed under a second condition using the same beam size but a high current (see below). For Cl, counting time was 60 s at peak and 30 s at both sides of background. For F, counting time was 120 s at peak and 60 s at background.

As described above, the PHA setting (which can completely eliminate the Mg overlap) was as follows: differential mode, baseline = 2800 mV, window = 1100 mV. Before performing the calibration to quantify the Fe overlap, the count rate stability of F with varying beam current and exposure time was checked by testing two reference materials that contained trace level F, i.e., Kakanui Hornblende (USNM 143965), and Rhyolitic glass VG-568 (USNM 7285). A beam size of 5 µm was used for the hornblende and a beam size of 10 µm was used for the glass, which is a practical compromise between obtaining sufficient resolution and reducing sample damage. As indicated by signal recording with time, the F count rate for the hornblende with a beam current of 20 nA, 100 nA and 180 nA was constant over 900 s (Figure 4a), allowing us to use a high beam current (180 nA) and a long counting time to determine very low concentrations of F. For the rhyolitic glass, the F count rate was constant with a beam current from 20 to 60 nA, but a systematic increase occurred in the first 300 s when using a beam current of 100 nA (Figure 4b). Therefore, for the calibration of C^F_{Fe} and X_{FeO} of F-free materials and the measurement of F-bearing materials, we used beam currents of 180 nA and 60 nA for minerals and glasses respectively.

In the following we provide some discussion on the phenomenon that a high beam current would result in an increase of the F signal with time for the rhyolitic glass (Figure 4b). Witter and Kuehner (2004) proposed that the

Table 3.
Summary of the recommended method for the measurement of trace level F

Step	Object	Operation	Recommended setting
1	F-rich reference material (e.g., fluorapatite)	Search for F*K*α peak position using PC1	–
2	F-free, Fe- and Mg-bearing reference material (e.g., hornblende)	Modify PHA setting to eliminate Mg X-ray signals	PHA integral mode, baseline = 2800 mV, window = 1100
3	F-free, Fe-bearing known minerals or glasses	Measure a series values of pseudo F concentrations (C^F_{Fe})	F*K*α peak as detected in step 1, background at sinθ = F*K*α peak + 0.01
4	$C^F_{Fe} = a + b * X_{FeO}$	Calculate *a* and *b* using measured values of C^F_{Fe} and X_{FeO} via linear regression	–
5	F-bearing, Fe-bearing unknown target minerals or glasses	Measure FeO(T) content (X_{FeO})	–
6	F-bearing, Fe-bearing unknown target minerals or glasses	Measure raw F concentration (C^F_{mea})	F*K*α peak as detected in step 1, background at sin θ = F*K*α peak + 0.01
7	$C^F_{Fe} = a + b * X_{FeO}$	Calculate C^F_{Fe} using calculated *a* and *b* (step 4) and measured X_{FeO} (step 5)	–
8	$C^F_{real} = C^F_{mea}$ - C^F_{Fe}	Calculate real F concentration (C^F_{real}) using measured C^F_{mea} (step 6) and calculated C^F_{Fe} (step 7)	–

Measurements for minerals or glasses should be performed separately. Steps 3-6 must be performed using the same analytical setting.

Table 4.
F-bearing reference samples analysed in this study in comparison with literature data

Sample	Note	FeO(T) (% *m/m*)	MgO (% *m/m*)	Cl ± *s* (μg g^{-1})		F ± *s* (μg g^{-1})	
				liter. data	This study	liter. data	This study
Hornblende (Kakanui)	USNM 143965	10.9	12.9	205 ± 22 [a] 240 ± 100 [b]	237 ± 10	1300 ± 800 [b]	1673 ± 51
Hornblende (Arenal)	USNM 111356	11.3	14.3	–	208 ± 17	–	361 ± 46
VG-2	USNM 111240/52	11.3	6.77	316 ± 19 [c] 329 ± 5 [d]	303 ± 20	334 ± 14 [e]	301 ± 19
VG-A99	USNM 113498/1	13.2	5.00	227 ± 20 [c] 271 ± 9 [d]	225 ± 14	709 ± 47 [e] 976 ± 4 [f]	874 ± 98
VG-568	USNM 7285	1.11	0.03	1013 ± 53 [g]	1045 ± 35	–	1968 ± 56
BCR-2G		12.4	3.59	98 ± 8 [h]	99 ± 18	448 ± 3 [h]	317 ± 59
AC-E glass	Au1030	2.11	0.01	162 ± 91 [h] 261 ± 22 [i]	292 ± 17	1807 ± 184[h] 1962 ± 93 [i]	1890 ± 64
GS-N glass	Au1030	2.97	2.09	349 ± 7 [h] 456 ± 32 [i]	497 ± 20	919 ± 5 [h] 932 ± 31 [i]	920 ± 38
DR-N glass	AuPd1200	8.18	4.36	545 ± 25 [i]	521 ± 23	567 ± 97 [i]	573 ± 71

Sources of literature data: [a]Wolff (2014); [b]Vanko (1986); [c]Thordarson *et al.* (1996); [d]van der Zwan *et al.* (2012); [e]Straub and Layne (2003). [f]Witter and Kuehner (2004); [g]Streck and Wacaster (2006); [h]Michel and Villemant (2003); [i]Wang *et al.* (2014). Analytical number was 10 for each sample. Note that the Cl and F literature data for BCR-2G were analysed for rock powders of BCR-2, while the glass BCR-2G was synthesised by the USGS via melting rock powders in platinum boats at 1350 °C in a 1-atm oven. AC-E, GS-N and DR-N glasses were synthesised from rock powders accordingly; 'Au1030' indicates that the glass was synthesised using a Au capsule (with extra ~ 5% *m/m* H_2O) and a melting temperature of 1030 °C, and 'AuPd1200' indicates the glass was synthesised using a AuPd capsule (without extra H_2O) at a melting temperature of 1200 °C.

increase of F counts might be a complex outcome involving beam-induced effects from both the loss of Na and K and the 'grow-in' of Si and Al (Morgan and London 1996). To test and clarify this observation, signal recording for Fe (Fe*L*α), Na, K, Si and Al was performed for the rhyolitic glass using a beam size of 10 μm and a beam current of 100 nA. The results are shown in Figure 5. First, the count rate for Fe (intensity of Fe*L*α with a PC1 pseudocrystal, see Figure 1a) showed no variation with time, indicating that the variation of count rate at the F*K*α peak is not related to the interference from Fe. Second, there were strong exponential signal decreases for both Na and K, and exponential signal increases for Si and Al, confirming the conclusion of Witter and Kuehner (2004). The co-variation pattern of the F signal with Si, Al, Na and K signals also implies that F in the glass structure might coordinate preferentially with Si and Al, but

not with Na or K, which is supported by structural studies in Si- and Al-rich glasses (e.g., Dingwell *et al.* 1985, Schaller *et al.* 1992).

Newly synthesised reference glasses

Because available reference glasses for F determination are very limited (see below), and to provide more useful microanalytical reference glasses with well constrained F contents, we synthesised glasses in a closed system from bulk rock powders of AC-E (granite), GS-N (granite) and DR-N (diorite), which have been regularly used as reference materials for bulk halogen analysis (see references in Table 4). For synthesising the glasses, two approaches were used using an internally heated pressure vessel (IHPV, Institute of Mineralogy, Leibniz University of Hannover) equipped with a rapid quench device (quench rate *ca.* 150 °C s^{-1}; see details in Berndt *et al.* 2002). In one approach, applied to AC-E and GS-N, rock powder test portions of *ca.* 0.2 g were placed in Au capsules with approximately 5% *m/m* H_2O (for the purpose of decreasing the liquidus of the system). The sealed capsules were then heated in an IHPV at 400 MPa and 1030 °C for about 3 d. No fluid phase was detected after the capsules were opened. Considering that the partitioning of F between fluid and melt is lower than that of Cl (e.g., Villemant and Boudon 1999), and that the measured Cl concentrations of the synthesised glasses were in good agreement with the literature data of the bulk powders (Table 4), we conclude that there was no loss of halogens in a fluid phase during the experimental treatment at high pressure and temperature. Examinations with backscattered electron images and electron probe microanalyses of the product glasses confirmed complete melting and homogenous composition. In the other approach applied to DR-N, rock powder test portions (*ca.* 0.2 g) were loaded into AuPd capsules without additional H_2O, and the sealed capsules were then heated in an IHPV at 200 MPa and 1200 °C for about 2 d. Examinations with backscattered electron images of the product glasses also confirmed complete melting and homogenous composition.

Results and discussion

Fluorine concentrations in reference materials

Using the method described above, we measured the F concentrations (strictly, *mass fractions*) of a series of reference materials, including the Kakanui Hornblende (USNM 143965), the Arenal Hornblende (USNM 111356), the VG-2 basaltic glass (USNM 111240/52), the VG-A99 basaltic glass (USNM 113498/1), the BCR-2G basaltic glass, the VG-568 rhyolitic glass (USNM 7285), and the other three newly synthesised glasses from AC-E (granite),

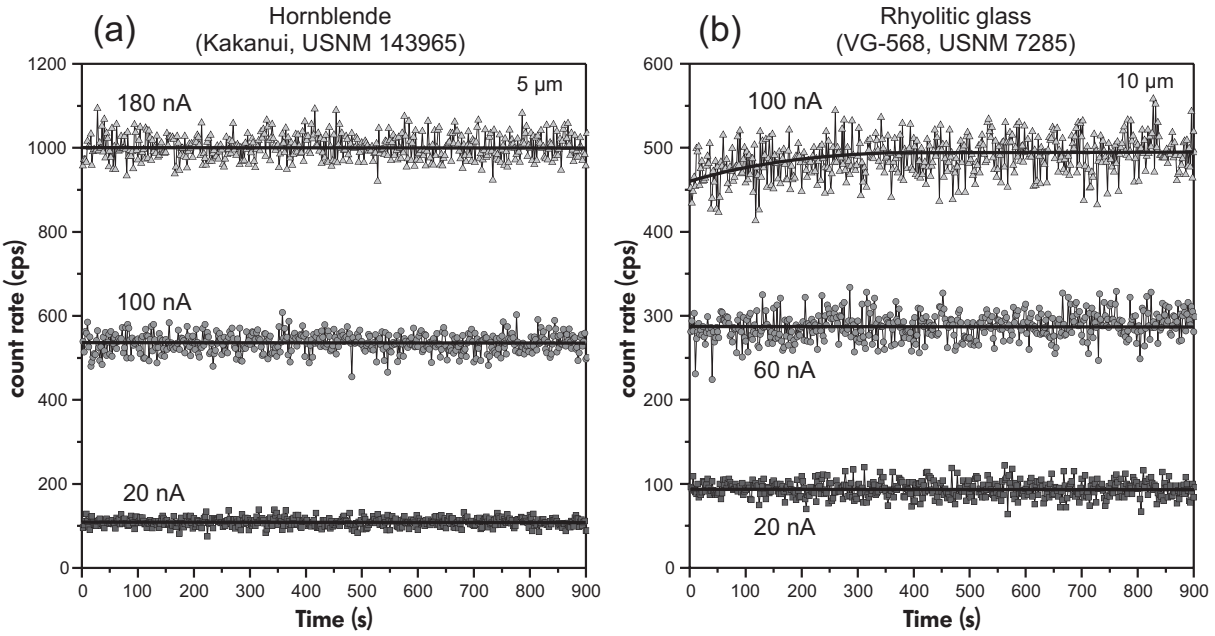

Figure 4. Record of count rate with time at the F*K*α peak for (a) Hornblende (Kakanui, USNM 143965) and (b) Rhyolitic glass (VG-568, USNM 7285). Note that, when using a beam current of 100 nA, the gross count rate at the F*K*α peak for the rhyolitic glass showed an apparent increase over the first 300 s.

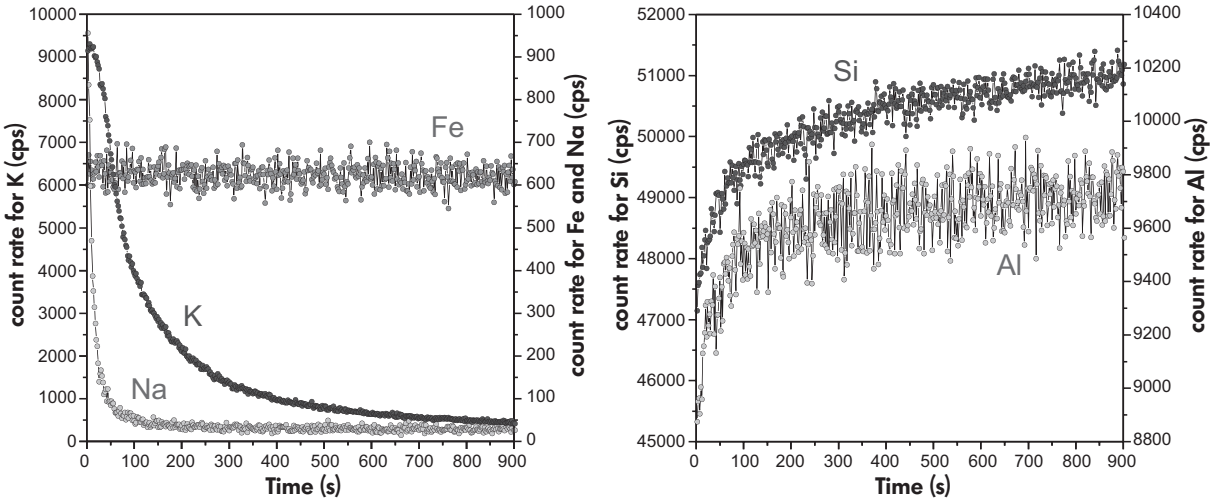

Figure 5. Record of the count rate with time for Fe, Na, K, Si, Al in a rhyolitic glass (VG-568, USNM 7285). Beam size was 10 μm and beam current was 100 nA. Diffraction crystals are PC1 (Fe), thallium acid phthalate (Na, Al, Si) and LPET (K).

GS-N (granite) and DR-N (diorite) powders. Table 4 shows their F concentrations (as well as FeO(T), MgO and Cl contents) determined in this study, which are plotted in comparison with literature data in Figure 6.

The F concentration of the widely used reference mineral Kakanui Hornblende determined in this study (1673 ± 51 μg g^{-1}) cannot be directly compared with the value published by Vanko (1986) (1300 ± 800 μg g^{-1}), which was measured using the TAP crystal that has a much lower count rate than with the PC1 pseudocrystal. Although Vanko (1986) used a high beam current of 250 nA (counting time of 60 s on peak and 30 s on both side background), the detection limit of F was reported as high as 700 μg g^{-1}, which should have resulted in the large uncertainty. It is remarkable that the newly measured concentration is much lower than the data previously determined with the PC1 pseudocrystal but without a careful treatment of the Mg and Fe overlaps (e.g., 3460 ± 50 μg g^{-1}, Zhang *et al.* 2012; 3666 ± 222 μg g^{-1}, Wolff 2014), emphasising the significance of the spectral interferences. Another reference mineral that is often used is Arenal Hornblende (USNM 111356), which was determined to contain 361 ± 46 μg g^{-1} F (this study). Because of the lack of accurate F data in the literature for these commonly used reference minerals, the accuracy of this method applied to minerals cannot be ascertained at present and should be tested with other analytical techniques.

The F mass fraction of the natural reference basaltic glass VG-2 analysed in this study was 301 ± 19 μg g^{-1}, which is in agreement within error with the value (334 ± 14 μg g^{-1}) determined using ion probe by Straub and Layne (2003). The literature data for the natural reference basaltic glass VG-A99 show a relatively broad range of F values, including 709 ± 47 μg g^{-1} determined using ion probe by Straub and Layne (2003), and 976 ± 4 μg g^{-1} determined by Witter and Kuehner (2004) using EPMA with a calibration.

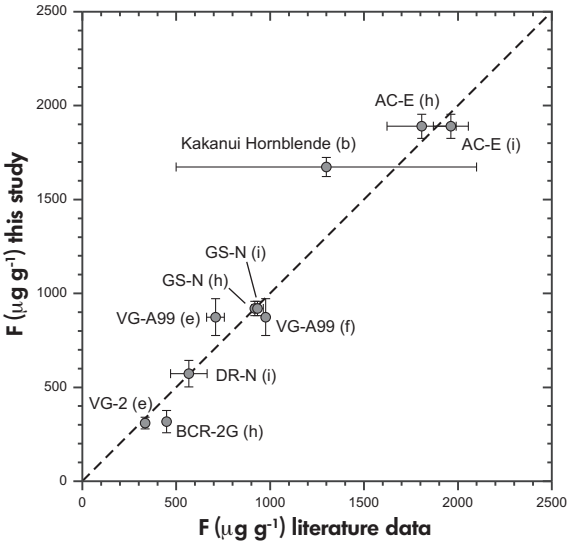

Figure 6. Comparison of F mass fractions in literature data and in this study. Each point is marked with the sample name and the source of literature data in given brackets (see corresponding source in Table 4). The dashed line is the 1:1 line.

This difference may reflect sample heterogeneity and/or different analytical accuracy. Our method yielded a value of 874 ± 98 μg g^{-1}, which is within the range of literature data. In addition, no value for F in the reference rhyolitic glass VG-568 has been reported in the literature to the best of our knowledge, and we obtained a value of 1968 ± 56 μg g^{-1}.

The basaltic glass BCR-2G was synthesised by the USGS by melting rock powders of BCR-2 basalt in platinum boats at 1350 °C in a 1-atm oven (Stephen Wilson, USGS, pers. comm. 2015). However, melting in an open environment may change the concentration of volatile elements from the original rock powder as a result of degassing. Michel and Villemant (2003) applied pyrohydrolysis and ion chromatography to determine volatile elements in the natural basalt powder BCR-2, and obtained 448 ± 3 μg g^{-1} F. In this study, F in the synthesised glass BCR-2G was measured to be 317 ± 59 μg g^{-1}. This value is apparently lower than that determined in the bulk powder by Michel and Villemant (2003), and the difference probably results from degassing during the synthesis of the glass. Therefore, we suggest that the BCR-2G glass may not be a suitable reference material for the determination of F.

The Cl concentrations of the synthesised glasses from AC-E, GS-N and DR-N rock powders are nearly consistent within error with the literature data for bulk powders (Table 4), demonstrating the reliability of our approach to glass synthesis at high pressure in a closed system. The F values derived for all three synthesised glasses are consistent within error with the literature data measured for the original rock powders. Considering the limited number of available reference glasses with well-constrained F data, the synthesised AC-E, GS-N and DR-N glasses may serve as reference materials and/or measurement standards for microanalysis of F in glasses.

Detection limit and uncertainty

Theoretically, a 'detection limit' refers to a lowest concentration that corresponds to a spectral peak that can be distinguished from statistical background fluctuations. The value of a detection limit is recommended to be that corresponding to a peak count higher than the mean background count by three times of standard deviation of background count (Analytical Methods Committee 1987). Practically, for the method presented above, we can easily obtain detection limits from the analytical results of F-free materials used for calibrating the Fe overlap (see Table 2), because the fluctuations of pseudo F concentrations of the F-free materials correspond to the practical fluctuations of the background for analysing F-bearing materials. The standard deviations for minerals and glasses listed in Table 2 are thus averaged for calculating statistical detection limits. As a result, the detection limit for minerals using a 180-nA beam current (counting time: 120 s at peak and 60 s at background) is calculated to be 82 μg g^{-1} F, and the detection limit for glasses using a 60-nA beam current (counting time: 120 s at peak and 60 s at background) is calculated to be 106 μg g^{-1} F.

The method using the PC1 pseudocrystal described above significantly improved the analytical accuracy for F determination compared with using the TAP crystal, but may meanwhile lower the precision by introducing extra uncertainty derived from linear regression for calibrating the Fe overlap (i.e., the relation between C^F_{Fe} and X_{FeO}). However, as indicated by the results of the linear regression shown in Figure 3, such additional uncertainty should be very limited because the coefficient of determination (R^2) is very close to 1. Based on the measurements of this study, we found that the additional uncertainty, which can be potentially derived from linear regression, is negligible compared with the statistical uncertainty of C^F_{mea} (directly given by the instrument) and thus neglected when reporting the final results of C^F_{real} (Table 4).

Conclusions

The count rate of fluorine can be significantly improved by using the W-Si multi-layered (PC1) pseudocrystal compared with using the TAP crystal, but this method introduces spectral interferences of Mg and Fe X-ray lines with the F*K*α line. The two-step method described in this study was successful (a) in eliminating the Mg overlap by adjusting the PHA setting and (b) in calibrating quantitatively the Fe overlap by measuring a series of Fe-bearing but F-free materials. A beam current of 180 nA (with a 5-μm beam size) is appropriate for measuring F in minerals, but a lower beam current of 60 nA (with a 10-μm beam size) is recommended for measuring F in glasses to avoid potential variation of count rate with time. The reliability of this approach was demonstrated using various reference materials with trace F contents. In addition, glasses synthesised at high pressure from powders of the rock reference materials AC-E, GS-N and DR-N are available as new reference materials for the determination of F by microbeam methods in glasses.

Acknowledgements

We thank Michael Marks (Universität Tübingen) for providing rock powders of AC-E, GS-N and DR-N, Martin Oeser for providing BCR-2G, and Tim Müller and Anna-Maria Welsch for helpful discussions. Special thanks go to Julian Feige for his perfect preparation of thin sections. This

paper benefited greatly from critical and constructive comments of two anonymous reviewers and the journal editors. This work was supported by a 'Wege in die Forschung' project (granted by Leibniz Universität Hannover to Chao Zhang), DFG projects KO 1723/17 and HO 1337/31. Requests for the newly synthesised AC-E, GS-N and DR-N glasses as microanalytical reference materials can be addressed to the corresponding author.

References

Analytical Methods Committee (1987)
Recommendations for the definition, estimation and use of the detection limit. **Analyst**, **112**, 199–204.

Anzelmo J.A. and Boyer B.W. (1987)
The analysis of carbon and other light elements using layered synthetic microstructures. **Advances in X-ray Analysis**, **30**, 193–200.

Berndt J., Liebske C., Holtz F., Freise M., Nowak M., Ziegenbein D., Hurkuck W. and Koepke J. (2002)
A combined rapid-quench and H_2-membrane setup for internally heated pressure vessels: Description and application for water solubility in basaltic melts. **American Mineralogist**, **87**, 1717–1726.

Beyer C., Klemme S., Wiedenbeck M., Stracke A. and Vollmer C. (2012)
Fluorine in nominally fluorine-free mantle minerals: Experimental partitioning of F between olivine, orthopyroxene and silicate melts with implications for magmatic processes. **Earth and Planetary Science Letters**, **337**, 1–9.

Chevychelov V.Y., Botcharnikov R.E. and Holtz F. (2008a)
Partitioning of Cl and F between fluid and hydrous phonolitic melt of Mt. Vesuvius at ~ 850–1000 °C and 200 MPa. **Chemical Geology**, **256**, 172–184.

Chevychelov V.Y., Bocharnikov R.E. and Holtz F. (2008b)
Experimental study of chlorine and fluorine partitioning between fluid and subalkaline basaltic melt. **Doklady Earth Sciences**, **422**, 1089–1092.

Dingwell D.B., Scarfe C.M. and Cronin D.J. (1985)
The effect of fluorine on viscosities in the system Na_2O-Al_2O_3-SiO_2: Implications for phonolites, trachytes and rhyolites. **American Mineralogist**, **70**, 80–87.

Donovan J.J., Snyder D.A. and Rivers M.L. (1993)
An improved interference correction for trace element analysis. **Microbeam Analysis**, **2**, 23–28.

Fialin M., Rbemy H., Richard C. and Wagner C. (1999)
Trace element analysis with the electron microprobe: new data and perspectives. **American Mineralogist**, **84**, 70–77.

Goldstein J.L., Newbury D.E., Echlin P., Joy D.C., Piori C.E. and Lifshin E. (1981)
Scanning electron microscopy and X-ray microanalysis. **Plenum (New York)**.

Jarosewich E., Nelen J.A. and Norberg J.A. (1980)
Reference samples for electron microprobe analysis. **Geostandards Newsletter**, **4**, 43–47.

Jercinovic M.J. and Williams M.L. (2005)
Analytical perils (and progress) in electron microprobe trace element analysis applied to geochronology: background acquisition, interferences, and beam irradiation effects. **American Mineralogist**, **90**, 526–546.

Le Voyer M., Asimow P.D., Mosenfelder J.L., Guan Y., Wallace P.J., Schiano P., Stolper E.M. and Eiler J.M. (2014)
Zonation of H_2O and F concentrations around melt inclusions in olivines. **Journal of Petrology**, **55**, 685–707.

Marks M.A.W., Wenzel T., Whitehouse M.J., Loose M., Zack T., Barth M., Worgard L., Krasz V., Eby G.N., Stosnach H. and Markl G. (2012)
The volatile inventory (F, Cl, Br, S, C) of magmatic apatite: An integrated analytical approach. **Chemical Geology**, **291**, 241–255.

Michel A. and Villemant B. (2003)
Determination of halogens (F, Cl, Br, I), sulfur and water in seventeen geological reference materials. **Geostandards Newsletter: The Journal of Geostandards and Geoanalysis**, **27**, 163–171.

Morgan G.B. VI and London D. (1996)
Optimizing the electron microprobe analysis of hydrous alkali aluminosilicate glasses. **American Mineralogist**, **81**, 1176–1185.

Potts P.J. and Tindle A.G. (1989)
Analytical characteristics of a multilayer dispersion element (2d = 60 A) in the determination of fluorine in minerals by electron microprobe. **Mineralogical Magazine**, **53**, 357–362.

Pouchou J.L. and Pichoir F. (1991)
Quantitative analysis of homogeneous or stratified microvolumes applying the model "PAP". **In: Heinrich K.F.J. and Newbury D.E. (eds), Electron probe quantitation. Plenum Press (New York, USA)**, 31–75.

Schaller T., Dingwell D.B., Keppler H., Knöller W., Merwin L. and Sebald A. (1992)
Fluorine in silicate glasses: A multinuclear nuclear magnetic resonance study. **Geochimica et Cosmochimica Acta**, **56**, 701–707.

Straub S.M. and Layne G.D. (2003)
The systematics of chlorine, fluorine, and water in Izu arc front volcanic rocks: Implications for volatile recycling in subduction zones. **Geochimica et Cosmochimica Acta**, **67**, 4179–4203.

Streck M.J. and Wacaster S. (2006)
Plagioclase and pyroxene hosted melt inclusions in basaltic andesites of the current eruption of Arenal volcano, Costa Rica. **Journal of Volcanology and Geothermal Research**, **157**, 236–253.

Thordarson T., Self S., Óskarsson N. and Hulsebosch T. (1996)
Sulfur, chlorine, and fluorine degassing and atmospheric loading by the 1783–1784 AD Laki (Skaftár Fires) eruption in Iceland. **Bulletin of Volcanology**, **58**, 205–225.

references

Vanko D.A. (1986)
High-chlorine amphiboles from oceanic rocks: Product of highly-saline hydrothermal fluids? **American Mineralogist, 71**, 51–59.

Villemant B. and Boudon G. (1999)
H_2O and halogen (F, Cl, Br) behaviour during shallow magma degassing processes. **Earth and Planetary Science Letters, 168**, 271–286.

Wang L.-X., Marks M.A.W., Keller J. and Markl G. (2014)
Halogen variations in alkaline rocks from the Upper Rhine Graben (SW Germany): Insights into F, Cl and Br behavior during magmatic processes. **Chemical Geology, 380**, 133–144.

Webster J.D. (1990)
Partitioning of F between H_2O and CO_2 fluids and topaz rhyolite melt. **Contributions to Mineralogy and Petrology, 104**, 424–438.

Webster J.D., Holloway J.R. and Hervig R.L. (1987)
Phase equilibria of a Be, U and F-enriched vitrophyre from Spor Mountain, Utah. **Geochimica et Cosmochimica Acta, 51**, 389–402.

Witter J.B. and Kuehner S.M. (2004)
A simple empirical method for high-quality electron microprobe analysis of fluorine at trace levels in Fe-bearing minerals and glasses. **American Mineralogist, 89**, 57–63.

Wolff P.E. (2014)
Hydrothermal circulation from very high to low temperatures in the lower oceanic crust: Evidence from layered gabbros from the Oman ophiolite and from partial melting experiments on oceanic gabbros. **PhD thesis, University of Hannover**, 167pp.

Zhang C., Holtz F., Ma C., Wolff P. and Li X. (2012)
Tracing the evolution and distribution of F and Cl in plutonic systems from volatile-bearing minerals: A case study from the Liujiawa pluton (Dabie orogen, China). **Contributions to Mineralogy and Petrology, 164**, 859–879.

van der Zwan F.M., Fietzke J. and Devey C.W. (2012)
Precise measurement of low (< 100 ppm) chlorine concentrations in submarine basaltic glass by electron microprobe. **Journal of Analytical Atomic Spectrometry, 27**, 1966–1974.

Supporting information

The following supporting information may be found in the online version of this article:

Table S1. Composition of synthesised F-free amphiboles and glasses.

This material is available as part of the online article from:http://onlinelibrary.wiley.com/doi/10.1111/j.1751-908X.2015.00390.x/abstract (This link will take you to the article abstract).

